

Arbitrarily loss-tolerant Einstein-Podolsky-Rosen steering allowing a demonstration over 1 km of optical fiber with no detection loophole

A. J. Bennet,^{1,2} D. A. Evans,^{1,2} D. J. Saunders,^{1,2} C. Branciard,³
E. G. Cavalcanti,² H. M. Wiseman,^{1,2,*} and G. J. Pryde^{1,2,†}

¹Centre for Quantum Computation and Communication Technology (Australian Research Council),
Griffith University, Brisbane, Queensland 4111, Australia

²Centre for Quantum Dynamics, Griffith University, Brisbane, Queensland 4111, Australia

³School of Mathematics and Physics, University of Queensland, Brisbane, Queensland 4072, Australia

Whether for quantum cryptography or for testing fundamental properties of the universe, it will be essential to demonstrate nonclassical effects over longer and longer distances. The chief barrier to doing so is loss of photons during propagation, because considering only those cases where a photon is detected opens a “detection loophole” in the security of any quantum information task in which parties or devices are untrusted. EPR-steering is a nonclassical effect which allows one party to verify that he shares entanglement with another party, even though he doesn’t trust her. We present the surprising and practical result that EPR-steering can be demonstrated with the detection loophole closed even in the presence of arbitrary losses, by using new loss-tolerant tests based on a sophisticated measurement strategy. We perform the first detection-loophole-free demonstration of EPR-steering with entangled photon pairs. We demonstrate that this can be extended to high loss, in an experiment where the parties are separated by a coiled 1 km optical fiber, giving total losses of 8.9 dB (87%).

In quantum mechanics, when two particles are in a pure entangled state, a measurement of one (say, Alice’s) induces an apparent nonlocal collapse of the state of the other (Bob’s), as first discussed by Einstein, Podolsky and Rosen (EPR) [1]. This nonclassical phenomenon was called “spooky action at a distance” by Einstein [2], and “steering” by Schrödinger [3]. Schrödinger realized that with a maximally entangled state, for any given observable Bob chooses to measure, Alice can, by an appropriate choice of her own measurement, “steer” Bob’s state into an eigenstate of his observable and thus predict its outcome [3]. The recent formalization [4] of “EPR-steering” [5] as a quantum information task further generalizes Schrödinger’s notion by allowing for mixed states and imperfect measurements.

In the EPR-steering task, Alice tries to convince Bob, who does not trust her, that they share pairs of entangled quantum particles [6]. The protocol proceeds by Alice and Bob comparing results from rounds of local “measurement” on each pair of particles. Bob’s measurement is always genuine, but he cannot assume that Alice’s is—a dishonest Alice may instead try to cheat. The only way for an honest Alice to distinguish herself is by her ability to steer Bob’s state. A dishonest Alice may employ powerful cheating strategies which to Bob would appear indistinguishable from loss. For this reason Bob cannot simply ignore cases when Alice does not (or claims not to) detect a photon. Thus there is a great challenge in verifying entanglement sharing with an untrusted party over a long distance; using high-efficiency detectors can only ever partly compensate for transmission losses. Nevertheless, we theoretically and experimentally show that it is possible to design and implement a protocol that closes the detection loophole in EPR-steering, even in

the presence of extremely large losses.

The formal procedure for Bob to be sure he has observed EPR-steering is formulated with qubits (quantum bits) as follows (Fig. 1): **1.** Bob receives his qubit. **2.** Bob announces to Alice his choice of measurement setting (labelled k) from a predetermined set of n observables. **3.** Bob records his measurement outcome and Alice’s declared result, $A_k \in \{-1, 1\}$. **4.** Steps **1–3** are reiterated to obtain the average correlation or *steering parameter* \mathcal{S}_n , as defined in Eq. 1 below. **5.** If \mathcal{S}_n is larger than a certain *EPR-steering bound* C_n , i.e. if it violates the *EPR-steering inequality* $\mathcal{S}_n \leq C_n$, Alice has demonstrated EPR-steering.

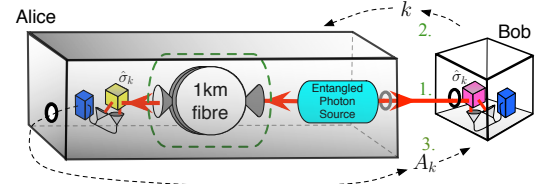


FIG. 1: Conceptual representation of the EPR-steering task. In each round of the protocol, **1.** Bob receives a photonic qubit, **2.** announces a measurement setting, k , and **3.** receives a “measurement” result from Alice—see text for details. Bob must assume that Alice controls the source, her line, and her detectors (all enclosed in the grey box). Bob implements the measurement $\hat{\sigma}_k$ (pink cube) and monitors the measurement outcome (blue box). In the case of an honest Alice, Bob’s qubit is half of an entangled pair and Alice’s measurement results are genuine; Alice measures in the same direction as Bob (yellow cube) using an identical apparatus. We demonstrate EPR-steering over 1 km of optical fiber inserted in the line on Alice’s side (green dashed box).

The obvious strategy for Alice to cheat is to send Bob, in each round, a single qubit in an eigenstate of one (chosen at random) of the n observables, and then decline to announce a measurement result whenever her observable does not correspond to Bob’s announced measurement. In this way, she can mimic the perfect correlations of an entangled state on those trials where she announces a result. Bob cannot be sure whether her unannounced results are due to cheating, or to genuine loss of her qubit, e.g. by photon absorption or scattering in transmission. He can only infer entanglement from the correlations if he makes a *fair sampling assumption*, that Alice’s loss events were independent of his setting. This assumption cannot be made if Alice is untrusted, opening up a so-called “detection loophole” [7]. Consequently, even if an untrusted Alice is honest, the protocol just described cannot be used by Bob to verify entanglement with her, or to test rigorously Einstein’s “spooky action”, over a long distance channel where losses are large.

This detection loophole in EPR-steering is in exact analogy to that for Bell inequalities [8]. The latter are similar to EPR-steering inequalities except that *neither* Alice *nor* Bob are trusted [4]. Note that the detection apparatus is part of a “party”; unless the apparatus is trusted, the party cannot be. Bell inequality violations have been demonstrated experimentally [9–12], albeit with the fair-sampling assumption, or other loophole-opening assumptions [7, 13–15]. Violating an EPR-steering inequality is easier than violating a Bell inequality, but harder than witnessing entanglement (with trusted parties) [4]. This hierarchy has previously been demonstrated experimentally both in terms of how noise-tolerant these tests are [6] and in terms of how simple they can be made (minimizing the number of distinct outcomes) [16]. We note however that both of these experiments also used the fair sampling assumption.

EPR-steering has previously been demonstrated in optical systems without making the fair sampling assumption, by making use of the high-efficiency detectors that exist for homodyne detection [17, 18]. However, unlike the protocols we introduce and demonstrate here, those protocols using two-mode squeezed states and quadrature measurements, in which Alice gets a result every time, cannot be used for high-loss situations. The reason is simple: if the channel losses are greater than 50%, then an untrusted Alice could, as far as Bob knows, actually have a zero loss channel, and be using a 50:50 beam-splitter to effect a simultaneous measurement of both quadratures. Such a dual measurement would allow Alice to choose after-the-fact which quadrature to report as having been measured, with no actual measurement choice on her part. But measurement choice by Alice is essential to any demonstration of EPR-steering. In fact this limit of 50% loss holds no matter how many different quadratures Alice may measure — see Sec. VI of ref. [19]. By contrast, the photonic protocol we demonstrate works

for losses much larger than 50%.

Nonclassical effects such as Bell nonlocality and EPR-steering not only illuminate fundamental issues in quantum mechanics [20]; they also have direct applications in quantum technology. For instance, the security of quantum key distribution (QKD) systems requires the existence of a channel that can transmit entanglement [21]. Further, the violation of a Bell inequality proves the existence of such a channel with no need for any assumptions about the devices involved. This allows for *device-independent* (DI) secure QKD: the two parties can establish a secret key even if they bought their equipment from an adversary [22]. Bob’s ability to verify entanglement via EPR-steering provides a similar resource for quantum communication.

Specifically, it has recently been shown [23] that performing an EPR-steering task allows for one-sided DI secure QKD, appropriate when Bob (at a fixed base station, say) can trust his detection apparatus, but cannot trust that of Alice (a roaming agent). That is, from the perspective of Bob, this entanglement verification is as strong as that from a Bell-inequality violation [8]. In both cases, it is essential for the security of the protocol that there be *no detection loophole*. By contrast, the locality and freedom-of-choice loopholes are not important in the cryptography context, as it is a necessary assumption of security proofs that no information escapes from Alice’s or Bob’s lab unless they allow it.

In EPR-steering, Bob trusts his own apparatus, so he can discard those experimental runs where he fails to detect a photon without having to invoke an additional fair sampling assumption. Because Bob’s detector settings are known only to him prior to the detection of his photon, Alice cannot exploit the loss of Bob’s photon—either inside or outside his lab. However, Bob cannot trust any claims Alice makes about the propagation losses or the efficiency of her detectors. All that Bob knows is Alice’s *heralding efficiency* ϵ : the probability with which she *declares* a non-null measurement result conditional on Bob’s detection.

The key result of this paper is that Bob can close the EPR-steering detection loophole, even in the presence of arbitrarily high loss, by making two modifications to the EPR-steering task described above. First, he must calculate Alice’s heralding efficiency ϵ from the protocol data. Second, he must compute a new, ϵ -dependent bound $C_n(\epsilon)$ which the steering parameter \mathcal{S}_n must exceed to demonstrate EPR-steering. This procedure, described in detail in the appendix, involves determining Alice’s optimal “cheating strategy” for a given ϵ . Her optimal strategy comprises probabilistic combinations of deterministic strategies. Of course if Alice “cheats” like this she will not actually fool Bob, as she will not violate the EPR-steering inequality we derive.

For every set of n observables measured by Bob there will be a different EPR-steering inequality. Intuitively,

the most useful inequalities will result from measurements that are as different from one another as possible. For qubits, this suggests using measurement axes that are regularly spaced on the Bloch sphere, as in ref. [6]. For details, see Additional Information.

Bob's measurements are described using quantum observables—in this case Pauli matrices $\hat{\sigma}_k^B$ for $k \in \{1, \dots, n\}$ —but we make no assumption about Alice and thus represent her declared results by a random variable $A_k \in \{-1, 1\}$. Generalizing the inequalities derived in ref. [6], we derive bounds $C_n(\epsilon)$ such that when the experimental statistics, post-selected on Alice's conclusive results, violate the inequality

$$\mathcal{S}_n \equiv \frac{1}{n} \sum_{k=1}^n \langle A_k \hat{\sigma}_k^B \rangle \leq C_n(\epsilon), \quad (1)$$

this demonstrates EPR-steering *with no detection loophole*.

The strongest bounds $C_n(\epsilon)$ are, by definition, the highest correlations which Alice can achieve by using cheating strategies, in which she sends a known (to her) pure state $|\xi\rangle$ to Bob drawn from some ensemble which depends upon n and ϵ . To determine Alice's optimal cheating strategies, we first consider deterministic strategies, in which Alice's declaration of +1, -1 (or null) as a result is determined by the state she sends, and the setting k Bob specifies. For each state $|\xi\rangle$ sent to Bob, we give Alice the power to declare her outcome only if Bob requests a result for k within a particular subset (depending on ξ) containing m elements, and declare a null result for the remaining $n - m$. This gives an apparent efficiency $\epsilon = m/n$. For a given m , we call the set of states which allow Alice to maximize her correlation “cheating ensembles”. When Alice chooses states from a single cheating ensemble, she is employing a deterministic cheating strategy. In such a strategy, the optimal bound on \mathcal{S}_n that she can attain is given by

$$D_n(m) = \max_{\{A_k\}_m} \left\{ \lambda_{\max} \left(\frac{1}{m} \sum_k A_k \hat{\sigma}_k^B \right) \right\}, \quad (2)$$

where the maximisation is over sets $\{A_k\}_m$ where exactly m of the A_k take values ± 1 , while the rest are null (and can be taken to have value 0, for mathematical convenience). Moreover, performing the maximization reveals the optimal cheating ensemble, as each set $\{A_k\}_m$ for which the maximum λ_{\max} in eq. (2) is attained defines a state: the eigenstate corresponding to that λ_{\max} . Examples of such cheating ensembles are shown in Fig. 2, for $n = 10$ and $m \in \{2, 3, 4, 5\}$.

However, Alice does not necessarily have to choose strategies where exactly m out of her n measurements are non-null. Indeed, the optimal deterministic strategies just considered are not necessarily the optimal strategies for Alice even for an apparent efficiency such that ϵn is

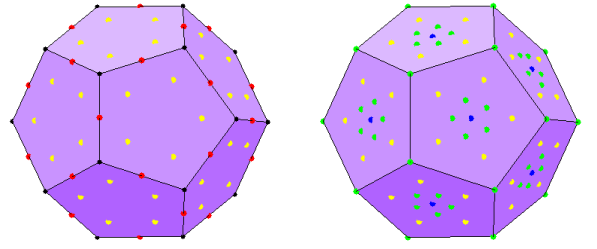


FIG. 2: **Alice's optimal cheating ensembles for $n = 10$ and $\epsilon \in [0.2, 0.5]$.** This figure shows, in Bloch space, the directions of the states in Alice's optimal “cheating ensembles” that set the bound $C_n(\epsilon)$ for EPR-steering when $\epsilon \in [0.2, 0.3]$ (on the left) and when $\epsilon \in [0.3, 0.5]$ (on the right), for the exemplary case of $n = 10$. The black dots (only visible on the left) define Bob's measurement axes: the vertices of the dodecahedron. For the deterministic strategy where Alice gives non-null results for only two of Bob's settings ($m = 2$), the red dots (on the left) define the optimal states Alice should send, and likewise for $m = 3$ (yellow; both), $m = 4$ (green; right) and $m = 5$ (blue; right). For any heralding efficiency $0.2 < \epsilon < 0.3$ (left) Alice's optimal strategy is nondeterministic: a mixture of the $\epsilon = 0.2$ strategy (red) and the $\epsilon = 0.3$ strategy (yellow). For any $0.3 < \epsilon < 0.5$ (right) a dishonest Alice should use a mixture of the $\epsilon = 0.3$ (yellow) and $\epsilon = 0.5$ (blue) strategies. Interestingly, the $m = 4$ (green) deterministic strategy is *never* used; this is seen also in Fig. 3 (where the corresponding point does not lie on the curve representing the optimal strategy).

an integer m , and clearly do not apply if ϵn is not an integer. For any ϵ , we must consider Alice's most general strategy: a probabilistic mixture of optimal deterministic strategies of different m , with weights w_m . Because we are considering linear inequalities, the bound yielded by this strategy for any ϵ is simply

$$C_n(\epsilon) = \max_{\{w_m\}} \left[\sum_{m=1}^n w_m D_n(m) \right], \quad (3)$$

with the constraints $0 \leq w_m \leq 1$, $\sum_{m=1}^n w_m = 1$, and $\sum_{m=1}^n (m/n) w_m = \epsilon$. By linearity, the maximum is achieved with at most two nonzero w_m s, so the bound $C_n(\epsilon)$ can easily be evaluated numerically for any finite set of observables.

The theoretical values for $C_n(\epsilon)$ are shown in Fig. 3. As expected, $C_n(\epsilon)$ monotonically decreases with ϵ ; the $\epsilon = 1$ bounds correspond to those derived in ref. [6]. The key point is that, for any arrangement of n different measurement settings, it is possible to steer using a maximally entangled state if and only if $\epsilon > 1/n$. This is because \mathcal{S}_n can reach its maximum value of 1 with maximally entangled states, while the only way for Alice to obtain $\mathcal{S}_n = 1$ by cheating would be to send a state aligned perfectly with one of Bob's measurement directions, and giving a null result for the other $n - 1$ settings. Thus, it becomes possible to demonstrate steering even with arbitrarily high losses, as long as Alice and Bob em-

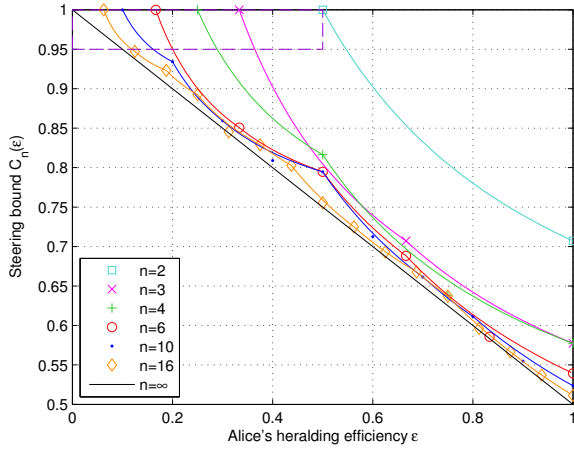


FIG. 3: Loss-dependent EPR-steering bounds. The solid curves are the theoretical bounds $C_n(\epsilon)$ on \mathcal{S}_n for demonstrating EPR-steering with no detection loophole, for $n = 2, 3, 4, 6, 10, 16$, and ∞ . The same-coloured symbols (some of which do not lie on the curves) correspond to the steering parameter \mathcal{S}_n theoretically obtainable by a cheating Alice using a deterministic strategy.

ploy a sufficiently elaborate, many-setting, measurement scheme. Indeed it can be shown (see appendix) that for an infinite number of measurements ($n = \infty$) uniformly distributed on the Bloch sphere, $C_\infty(\epsilon) = 1 - \frac{1}{2}\epsilon$. That is, there is a gap between the maximum quantum correlation, $\mathcal{S}_\infty = 1$, and the EPR-steering bound $C_\infty(\epsilon)$ for any $\epsilon > 0$.

We experimentally demonstrated detection-loophole free EPR-steering using photonic Bell states generated from an efficient spontaneous parametric down-conversion (SPDC) source—namely, a polarisation Sagnac interferometer, based on refs. [24, 25] (see Fig. 4). Note that in a genuine quantum communication context, Bob must choose his setting independently from one shot to the next. For the purposes of our demonstration this level of rigour was not imposed. In addition, since we (the experimenters), control Alice’s implementation of honest or dishonest strategies, there is no need to force a time ordering of events 1–3. In a field deployment, the protocol would require a strict time ordering, which could be enforced using an optical delay line for Alice.

We implemented the n -setting measurement schemes for $n = 3, 4, 6, 10$ and 16 , and our experiments yielded values $\mathcal{S}_n \approx 0.99$ for each case (see Fig. 5). This gives an absolute ($n = \infty$) lower bound on Alice’s required heralding efficiency of $\epsilon \approx 0.02$. Our source and detector configuration achieved a maximum heralding efficiency of $\epsilon = 0.354 \pm 0.001$, far above our minimum requirement of 0.02 , enabling us to demonstrate EPR-steering for $n = 3$ and greater (Fig. 5), with no detection loophole.

We also approached the EPR-steering protocol experimentally from the point of view of a dishonest Alice. We

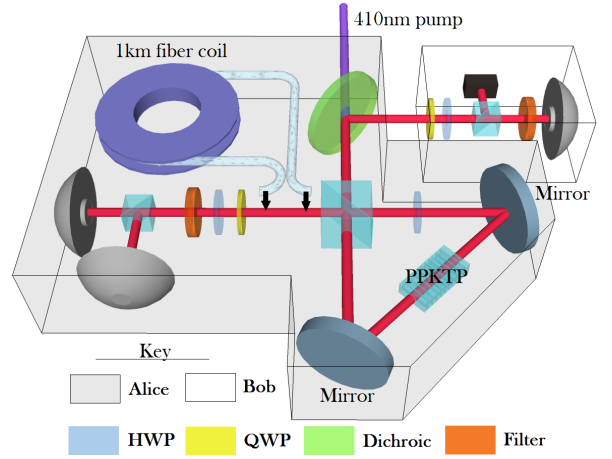


FIG. 4: Schematic of the experimental apparatus for demonstrating EPR-steering with no detection loophole. Bob’s apparatus is contained within the white box, while everything else, including the source, is assumed by Bob to be Alice’s (grey box) as per Fig. 1. A CW laser pumps a 10mm long periodically-poled KTP (PPKTP) crystal creating the maximally entangled singlet state. Measurement settings depend on the orientation of half- and quarter-wave plates (HWP/QWP), mounted in motorised rotation stages, relative to the axes of polarising beam splitters (PBSs), blue cubes. After filtering, photons are coupled to single-mode fibers leading to single-photon-counting modules and counting electronics. For some experiments, we insert a 1 km fiber coil between Alice’s detection apparatus and the source. Because Bob trusts his own apparatus, it is sufficient for him to use only one detector (grey hemisphere), corresponding to one (varied at random) of the two eigenstates of his observable $\hat{\sigma}_k^B$.

implemented Alice’s optimal cheating strategies, which were determined as described above. We find experimentally that Alice could indeed come close to saturating the bounds $C_n(\epsilon)$. See Fig. 5, Fig. 6. The small discrepancies between the measured $\mathcal{S}_n^{\text{cheat}}$ and the theoretical bound $C_n(\epsilon)$ arise from slightly imperfect state preparation and measurement settings.

Demonstrating transmission of entanglement over a channel such as an optical fiber is important for real-world applications such as one-sided DI secure QKD. If the entangled source were close to Alice, losses in the line would not be a problem because Bob can post-select on his detected events. But if this were not the case, for instance if Alice were a mobile field agent and the entangled source were at a base station, line losses to Alice would be critical and loss-tolerant protocols such as ours must be used.

Transmission through a single-mode optical fiber causes the additional problems of polarisation mode dispersion (PMD) [26] and uncompensated birefringence, which reduce \mathcal{S}_n . Thus to test the robustness of our protocol we inserted 1 km of single-mode fiber between

the Alice-side output of the Sagnac interferometer and Alice’s measurement apparatus (see Fig. 4). This introduced additional losses of 4.3 dB, and for our source we found $\epsilon = 0.132 \pm 0.001$ for $n = 10$ and $\epsilon = 0.130 \pm 0.001$ for $n = 16$. We successfully demonstrated EPR-steering with this setup, observing $\mathcal{S}_{10} = 0.985 \pm 0.006$ and $\mathcal{S}_{16} = 0.981 \pm 0.006$ (Fig. 5), 2.6 and 5.3 standard deviations above $C_{10}(\epsilon)$ and $C_{16}(\epsilon)$ respectively. Based on the intrinsic fiber losses, we estimate that it would still be possible to accomplish the EPR-steering task—with the detection loophole closed, with $n = 16$ measurement settings and with all other experimental parameters the same—through ~ 2 km of single-mode optical fiber. Thus we can see that an honest Alice can convince Bob that they share entanglement, even in the presence of very significant photon losses.

For the first time, we have closed the detection loophole in a photonic quantum nonlocality experiment. Unlike earlier demonstrations using continuous variable systems, our photonic protocol works with arbitrarily large transmission losses. Specifically, the novel EPR-steering inequalities we derived allow for arbitrarily low heralding efficiency. We demonstrated the violation of such inequalities over a 1 km optical fiber, with a heralding efficiency for Alice of -8.9 dB (13%). This demonstration used a large number (up to 16) of different measurement settings for the two parties and high fidelity entangled states. Increasing the number of settings, the state fidelity, or Alice’s detection efficiency, would allow for demonstrations of the EPR effect over substantially longer distances.

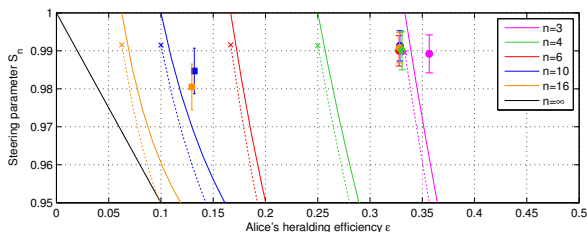


FIG. 5: Experimental Demonstration of EPR-Steering. A zoomed-in section of Fig. 3 (dashed purple box) with experimental data included. The data points show the experimental values for the steering parameter \mathcal{S}_n obtained for $n = 3, 4, 6, 10$ and 16 measurement settings. The \bullet points represent data straight from the entangled source, prior to the fiber being installed. The \blacksquare points (for $n = 10$ and 16 only) represent data collected after the single mode fiber was installed, demonstrating loss-tolerant EPR-steering with a transmission distance of 1 km. The error bars (one standard deviation) take into account systematic measurement errors and Poissonian photon counting noise. The \times points are experimental cheating data (shown in detail in the appendix), from which we derive our Alice’s closest approach using a cheating strategy (dashed curves).

The ability to keep the EPR-steering detection loophole closed with large losses opens new possibilities for security in long-range transmission of photonic entanglement over optical fiber, through free space [27] or to a satellite [28]. This has potential applications in cryptography, as well as allowing tests of Einstein’s “spooky action” over unprecedented distances.

We thank Matthew Palsson, Alessandro Fedrizzi and Devin Smith for helpful discussions. This research was conducted by the Australian Research Council Centre of Excellence for Quantum Computation and Communication Technology (Project number CE110001027).

ADDITIONAL INFORMATION

Defining the n measurements. We use measurements that are aligned, in Bloch space, as regularly as possible. For $n = 3, 4, 6$, and 10 this means using the the vertex-to-vertex axes of the Platonic solids (octahe-

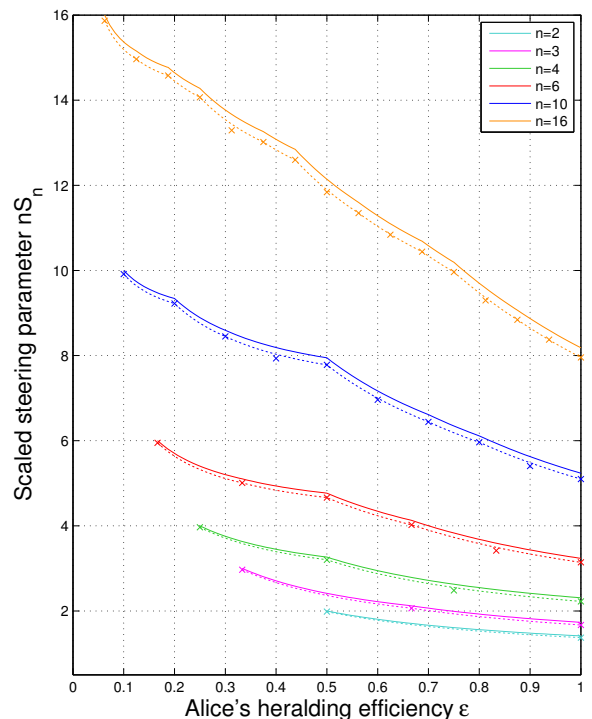


FIG. 6: **Experimental data for a dishonest Alice.** The solid curves are the bounds $C_n(\epsilon)$ on \mathcal{S}_n , for $n = 2, 3, 4, 6, 10$ and 16 . The vertical axis shows a scaled version of the steering parameter, $n\mathcal{S}_n$, purely for clarity when comparing the different bounds. The same-coloured \times ’s correspond to the experimentally observed steering parameter $\mathcal{S}_n^{\text{cheat}}$ obtained by a cheating Alice using a deterministic strategy. The dashed lines, derived from the data points, show the maximum $\mathcal{S}_n^{\text{cheat}}$ our Alice could achieve by combining two different deterministic strategies to simulate a heralding efficiency ϵ . Error bars are smaller than marker dimensions.

dron, cube, icosahedron and dodecahedron, respectively) with $2n$ vertices, as in ref. [6]. We also consider the case $n = 16$, for which we create a geodesic solid by combining the axes of the dodecahedron and its dual solid, the icosahedron. Note that we neither claim nor require that these arrangements give the strongest tests of EPR-steering for a given n , and a given heralding efficiency ϵ .

Optical cheating strategies. Alice's optimal deterministic strategy for a given m is obtained by choosing the states and declarations to maximize the correlation of A_k with Bob's outcomes. For Alice to create an apparent efficiency that is not a multiple of $1/n$, she must use a non-deterministic, or *mixed* strategy. To achieve the optimal strategy in general it turns out that Alice need only ever mix two optimal deterministic strategies, with $m_1/n < \epsilon < m_2/n$. Note however that m_1 and m_2 are *not* necessarily the largest and smallest integers such that this equation holds, and that even if $\epsilon = m/n$ for some m , the optimal strategy may be mixed.

From Lemma 1 of ref. [4] it is known that the optimal cheating ensemble can be assumed to have the same symmetry as the measurement settings. For settings based around the Platonic solids, where the symmetry group maps any one of Bob's settings into any other setting, this implies that Alice's states are identically arranged around each of Bob's settings. This is seen in Fig. 2. As a consequence, since Alice chooses a state at random from her ensemble, the probability of Alice's claiming a null result is independent of Bob's setting. This is an obvious condition which Bob could place upon Alice's results (to be convinced that Alice's null results really are null results) and for less symmetric setting arrangements (such as the $n = 16$ arrangement) this is an additional condition which could restrict Alice's choice of cheating strategies. Such a restriction can only reduce the effectiveness of Alice's cheating strategy, thereby *lowering* the bound $C_n(\epsilon)$ on what she can achieve without entanglement. Thus any demonstration of EPR-steering without such a restriction would remain so with it.

Entangled Photon Source. Our source used a 1mW, grating stabilised, continuous wave, fiber-coupled 410 nm laser to pump a 10 mm-long periodically-poled KTP (PPKTP) crystal bidirectionally. The PPKTP crystal is embedded in the Sagnac interferometer [24, 25], giving rise to polarisation-entangled photon pairs at 820 nm. The Sagnac entangled source can achieve a high heralding efficiency ($\epsilon = 0.354 \pm 0.001$), because the collinear quasi-phase-matching of the PPKTP crystal provides SPDC modes that are approximately gaussian, so that efficient coupling to single mode fiber is possible. At one output (Alice's side), we use a high-transmission long pass filter to maximize source efficiency, while at the other output (Bob's side) we use a 2 nm interference filter to filter the photons and reject background light. A dichroic mirror separates the down conversion mode from

the pump mode in Bob's output arm. The outputs are coupled into single-mode fibers, and connected to Perkin Elmer single photon counting modules (SPCM-AQR-14-FC) and counting electronics. The silicon avalanche photo diodes have a quantum efficiency of approximately 50% at 820nm. Using a coincidence window of ~ 3 ns, a coincidence count rate of approximately 6000 counts per second is achieved. The measured contribution in the coincidence rate from double-pair SPDC emission events is very small, approximately 0.1 per second. The resultant two-photon entangled state (at 820 nm) required high fidelity with a maximally entangled state to ensure a high value of \mathcal{S}_n . Our tomographically reconstructed state [29] had a fidelity of 0.992 ± 0.002 with the ideal singlet state. For the single photon source (used in the experimental implementation of Alice's optimal cheating strategy, see below), one arm of a polarisation-unentangled critically phase matched type-I bismuth triborate downconversion source is used. This was pumped by a 60mW 410nm CW laser.

1 km transmission channel A 1 km long single-mode fiber at 820 nm (Thorlabs SM800-5.6-125) was introduced between Alice's output of the Sagnac interferometer and her measurement apparatus. As well as introducing loss, the fiber implements an unknown polarisation unitary operation due to fiber birefringence. We undo this unitary operation in two stages. First we correct the state in the Z basis using a polarisation fiber controller, creating the state $|\psi\rangle = \frac{1}{\sqrt{2}}(|10\rangle + e^{i\phi}|01\rangle)$. We set the phase, ϕ , to $\frac{\pi}{2}$ using a tilted half wave plate set at its optic axis. The slight decrease in the steering parameter over the transmission distance is due to a combination of fiber noise (e.g. polarisation mode dispersion causing decoherence [26]) and minor errors in performing the polarisation correction.

* Electronic address: H.Wiseman@griffith.edu.au

† Electronic address: G.Pryde@griffith.edu.au

- [1] Einstein A, Podolsky B, Rosen N (1935) Can quantum-mechanical description of physical reality be considered complete? *Phys. Rev.* 47:777.
- [2] Born M (1949) in *Natural Philosophy of Cause and Chance*, Oxford University Press, page 109.
- [3] Schrödinger E (1935) Discussion of probability relations between separated systems. *Proc. Camb. Phil. Soc.* 31:555.
- [4] Wiseman HM, Jones SJ, Doherty AC (2007) Steering, entanglement, nonlocality, and the Einstein-Podolsky-Rosen paradox. *Phys. Rev. Lett.* 98:140402.
- [5] Cavalcanti EG, Jones SJ, Wiseman HM, Reid MD (2009) Experimental criteria for steering and the EPR paradox. *Phys. Rev. A.* 80:032112.
- [6] Saunders DJ, Jones SJ, Wiseman H M, Pryde GJ (2010) Experimental EPR-steering using bell-local states. *Nat. Phys.* 76:845-849.

- [7] Pearle PM (1970) Hidden-variable example based upon data rejection. *Phys. Rev. D*. 2:1418.
- [8] Bell JS (1964) On the Einstein-Podolsky-Rosen paradox. *Physics* 1:195-200.
- [9] Aspect A, Dalibard J, Roger G (1982) Experimental test of Bell's inequalities using time-varying analyzers. *Phys. Rev. Lett.* 49:1804.
- [10] Tittel W, Brendel J, Zbinden H, Gisin N (1998) Violation of Bell inequalities by photons more than 10 km Apart. *Phys. Rev. Lett.* 81:3563.
- [11] Weihs G, Jennewein T, Simon C, Weinfurter H, Zeilinger A (1998) Violation of Bell's Inequality under strict Einstein locality conditions. *Phys. Rev. Lett.* 81:5039.
- [12] Rowe MA, *et al.* (2001) Experimental violation of a Bell's inequality with efficient detection. *Nature*. 409:791.
- [13] Grangier P (2001) *Nature* 409:774.
- [14] Branciard C (2011) Detection loophole in Bell experiments: How postselection modifies the requirements to observe nonlocality. *Phys. Rev. A*. 83: 032123.
- [15] Scheidl T, *et al.* (2010) Violation of local realism with freedom of choice. *Proc. Natl. Acad. Sci. USA*. 107:19708.
- [16] Saunders DJ, *et al.* (2011) Maximally parsimonious demonstrations of quantum nonlocality. arXiv:1103.0306.
- [17] Ou ZY, Pereira SF, Kimble HJ, Peng KC (1992) Realization of the Einstein-Podolsky-Rosen paradox for continuous variables. *Phys. Rev. Lett.* 68:3663.
- [18] Bowen WP, Schnabel R, Lam PK, Ralph TC (2003) Experimental investigation of criteria for continuous variable entanglement. *Phys. Rev. Lett.* 90:043601.
- [19] Jones SJ, Wiseman HM (2011) Nonlocality of a single photon: paths to an EPR-steering experiment *Phys. Rev. A* 84:012110.
- [20] Oppenheim J, Wehner S (2010) The uncertainty principle determines the nonlocality of quantum mechanics. *Science* 19:1072.
- [21] Curty M, Lewenstein M, Lütkenhaus N (2004) Entanglement as a precondition for secure quantum key distribution. *Phys. Rev. Lett.* 92:217903.
- [22] Acín A, *et al.* (2007) Device-independent security of quantum cryptography against collective attacks. *Phys. Rev. Lett.* 98:230501.
- [23] Branciard C, Cavalcanti EG, Walborn S, Scarani V, Wiseman HM (2011) arXiv:1109.1435.
- [24] Kim T, Fiorentino M, Wong FNC (2006) Phase-stable source of polarization-entangled photons using a polarization Sagnac interferometer *Phys. Rev. A*. 73:012316.
- [25] Fedrizzi A, Herbst T, Poppe A, Jennewein T, Zeilinger A (2008) A wavelength-tunable fiber-coupled source of narrowband entangled photons *Opt. Expr.* 15:15377-15386.
- [26] Gordon JP, Kogelnik H (2000) PMD fundamentals: Polarization mode dispersion in optical fibers. *P. Proc. Natl. Acad. Sci. U.S.A.* 97:4541.
- [27] Ursin R, *et al.* (2007) Entanglement-based quantum communication over 144 km. *Nature Physics*. 3:481.
- [28] Aspelmeyer M, *et al.* (2003) Long-distance quantum communication with entangled photons using satellites. *IEEE J. Sel. Top. Quantum. Electr.* 9:1541.
- [29] James DFV, Kwiat PG, Munro WJ, White AG (2001) Measurement of qubits. *Phys. Rev. A* 64:052312.

Appendix

The following provides supplementary information on the derivation of the $C_n(\epsilon)$ bounds, of saturating the bounds using optimal cheating strategies, and a thorough analysis of the experimental error calculation of our data.

Derivation of the $C_n(\epsilon)$ bounds

As stated in the main text, Bob's measurements are described using quantum observables — in this case Pauli matrices $\hat{\sigma}_k^B$, oriented in the Bloch sphere along directions \mathbf{u}_k , for $k \in \{1, \dots, n\}$ — but we make no assumption about Alice and thus represent her declared results by a random variable $A_k \in \{-1, 1\}$.

In the idealised scenario where Alice declares a non-null result for all emitted pairs of systems, EPR-steering is demonstrated when the experimental statistics violate the linear inequality [5]

$$\mathcal{S}_n \equiv \frac{1}{n} \sum_{k=1}^n \langle A_k \hat{\sigma}_k^B \rangle \leq C_n, \quad (4)$$

where we call the correlation function, \mathcal{S}_n , the *steering parameter* for n settings, and C_n is the maximum value \mathcal{S}_n can attain if Bob has a pre-existing single-qubit quantum state known to Alice, rather than part of an entangled state. This bound is given by [6]

$$C_n = \max_{\{A_k\}} \left\{ \lambda_{\max} \left(\frac{1}{n} \sum_k A_k \hat{\sigma}_k^B \right) \right\}, \quad (5)$$

where $\lambda_{\max}(\hat{O})$ is the maximum eigenvalue of \hat{O} : C_n is derived by considering the maximum achievable correlation when Alice sends a known (to her) state $|\xi\rangle$ to Bob. Moreover, the eigenvectors associated with the λ_{\max} for every set $\{A_k\}$ that attains the maximum define the set of optimal states $\{|\xi_i\rangle\}$ which Alice can send to Bob in order to attain the bound. These are known as Alice's *optimal* “cheating ensemble” (though of course a dishonest Alice cannot actually cheat Bob). For two qubits, the maximum value of \mathcal{S}_n that can be achieved is unity, and this requires a maximally entangled state, while $C_n < 1$ for $n > 1$ as long as Bob's settings correspond to different observables.

If, on the other hand, Alice does not always declare a result $A_k \in \{-1, 1\}$ when requested, then she could be using her knowledge of Bob's state to post-select on her outcomes in a way that allows her to violate equation (4) even without entanglement. To illustrate how Alice could use an apparent inefficiency to her advantage, consider the situation where in each run Bob performs a measurement oriented along one of two (non-parallel) directions $\{\mathbf{u}_1, \mathbf{u}_2\}$. If Alice is not required to produce a result on every run, she could send with equal probability either a state with Bloch vector oriented along \mathbf{u}_1 or one oriented along \mathbf{u}_2 , and declare her result only if Bob asks her to reveal her result for A_1 or A_2 , respectively. Thus her apparent efficiency would be $\epsilon = 1/2$ and \mathcal{S}_2 would reach the maximum value of 1, whereas $C_2 < 1$. Alice would therefore be able to reproduce the correlations of an entangled state without any entanglement. This is the well-known detection loophole [7].

Thus, in realistic scenarios with loss, we need to take into account Alice's apparent efficiency ϵ and calculate a new bound $C_n(\epsilon)$, on the post-selected correlations, to replace C_n in equation (4), and which does not rely on a fair-sampling assumption for Alice. We derive such a bound by examining Alice's cheating strategies. We must consider the bounds on Alice's optimal deterministic strategies, and from them, construct Alice's optimal nondeterministic strategies, as demonstrated in the main article. Thus, Alice's optimal cheating ensembles are most often combinations of pairs of deterministic cheating ensembles.

Finally we consider the case $n \rightarrow \infty$, where Bob use infinitely many observables with uniform distribution on the sphere. Let $\theta \in [0, \pi]$ be the angle between Bob's measurement direction and the pure state $|\xi\rangle$ sent by a dishonest Alice, so that the expected correlation between Bob's result and what Alice reports is $|\cos(\theta)|$. Clearly if Alice is allowed an apparent efficiency ϵ , her optimal strategy is to report a non-null result only when $|\cos(\theta)| > \cos \Theta_\epsilon$, where Θ_ϵ is the half-angle of a cone which subtends a solid angle Ω satisfying $\Omega/4\pi = \epsilon/2$. That is, $\cos \Theta_\epsilon = 1 - \epsilon$. Using $d\Omega = d(\cos \theta) d\phi$, this optimal strategy gives a correlation, averaged over the cases where Alice gives a non-null report, of

$$C_\infty(\epsilon) = \frac{1}{\epsilon} \int_0^{2\pi} \frac{d\phi}{2\pi} \left\{ \int_{-1}^{-1+\epsilon} + \int_{1-\epsilon}^1 \right\} \frac{d(\cos \theta)}{2} |\cos(\theta)| = 1 - \frac{\epsilon}{2}. \quad (6)$$

Note that this is independent of the state Alice sends.

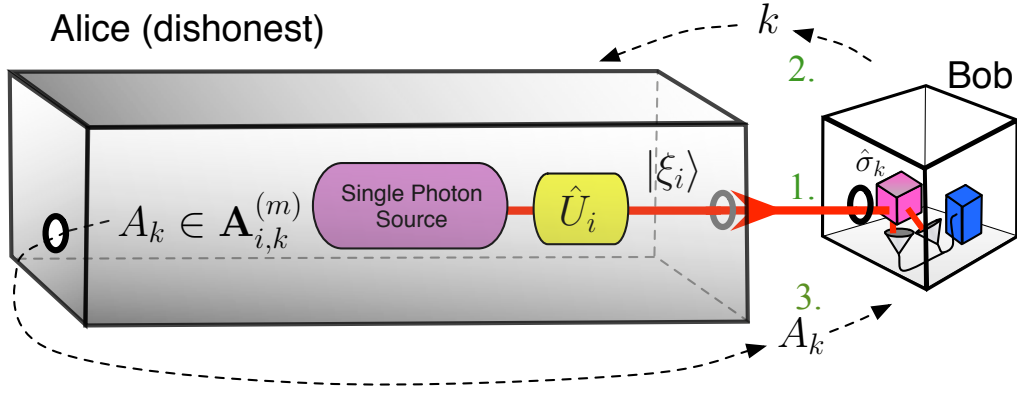


FIG. 7: **Conceptual representation of the EPR-steering task for a dishonest Alice.** (To be compared to Fig. 1 in the paper.) In each round of the protocol, **1.** Bob receives a photonic qubit, **2.** announces a measurement setting, k , and **3.** receives a “measurement” result from Alice. Bob must assume that Alice controls the source, her line, and her detectors (all enclosed in the grey boxes). In the case of a dishonest Alice, Alice’s optimal “cheating” strategy involves sending a single qubit prepared in a pure state $|\xi_i\rangle$ (using a single photon with a polarisation state prepared by the corresponding unitary \hat{U}_i), chosen from an optimal set. She announces a “measurement result” A_k , or a null result (announces nothing), from a look-up table $\mathbf{A}_{k,i}^{(m)}$ based on her preparation and Bob’s announced measurement direction. Note that the bounds for demonstrating EPR-steering, with no detection loophole, are set precisely to ensure that Alice cannot *actually* cheat — a dishonest Alice will fail to surpass the upper bound of any EPR-steering inequality.

Saturating the cheating bounds using a dishonest Alice

We experimentally generated the states in the optimal “cheating ensembles”, to test for correspondence between $C_n(\epsilon)$ and the maximal correlation $\mathcal{S}_n^{\text{cheat}}$ attainable by a dishonest Alice. The experimental apparatus for demonstrating Alice’s optimal cheating strategy (see Fig. S7) involved single qubit state preparation on Alice’s side, followed by single qubit measurement on Bob’s side. As mentioned earlier, Alice’s state preparation involved taking single photons from one arm of a polarisation-unentangled SPDC source. Single-qubit states encoded in polarisation were prepared using a PBS, HWP and QWP, and Bob’s measurement device was identical to that used in the case of genuine EPR-steering. The state preparation stage of the cheating experiment lets Alice send any pure state to Bob, while the measurement stage represents Bob’s ability to freely draw measurements from the set $\{\hat{\sigma}_k^B\}_n$, with $n = 3, 4, 6, 10$, and 16 , as in the case of genuine EPR-steering. Additionally, Bob can implement the $n = 2$ settings case, which corresponds to a pair of maximally complementary measurement settings. Alice prepares one of the $p(m)$ states in the optimal deterministic cheating ensemble $\{|\xi_i^{(m)}\rangle\}_{p(m)}$ each of which is (theoretically) equally good at enabling Alice to predict Bob’s outcome, given that she is obliged to give a non-null result only for m of Bob’s n settings. As explained above, for a given ϵ , Alice’s optimal strategy is usually a mixture of two different cheating ensembles (m' and m'' say), with weights $w_{m'}$ and $w_{m''} = 1 - w_{m'}$.

Therefore Bob’s observed $\mathcal{S}_n^{\text{cheat}}$ is predicted to be

$$\mathcal{S}_n^{\text{cheat}} = \frac{1}{n} \sum_{k=1}^n \sum_{m=m', m''} w_m \frac{1}{p(m)} \sum_{i=1}^{p(m)} \mathbf{A}_{k,i}^{(m)} \langle \xi_i^{(m)} | \hat{\sigma}_k^B | \xi_i^{(m)} \rangle \leq C_n(\epsilon). \quad (7)$$

Here $\mathbf{A}_{k,i}^{(m)} \in \{+1, 0, -1\}$ (stored as a look-up table, in which we treat a null result as 0) is the optimal announcement for Alice given that she has sent state $|\xi_i^{(m)}\rangle$ and Bob has announced that he is measuring along direction \mathbf{u}_k .

Experimental Error Calculation

In order to be sure that we have demonstrated EPR-steering, we need to know that the uncertainty in our measured \mathcal{S}_n is not so large as to make it possible that the true value would be less than the EPR-steering bound $C_n(\epsilon)$. By “true value” we mean the value that would be obtained if all of the assumptions that went into deriving the bound $C_n(\epsilon)$ were satisfied, namely that Bob’s measurements are perfect, and that the experiment yields the true quantum averages (which would require an infinite sample size). That is, we need to take into account (1) imperfection of Bob’s

measurements that could lead to an over-estimation of \mathcal{S}_n (systematic error), and (2) statistical errors in \mathcal{S}_n . These are determined in Parts 1 and 2 below, respectively. Note that we do not have to worry about systematic errors in Alice's measurement settings, since we make no assumptions about them in order to derive the EPR-steering bound.

Experimental error calculation, part 1: systematic error

In an ideal experiment, Bob's measurement corresponds to projecting his state onto one out of two orthogonal pure states, represented by opposite vectors \mathbf{u}_k and $-\mathbf{u}_k$ on the Bloch sphere. Bob's actual measurement will be nonideal in two ways. First, because the manufactured PBS has only a finite extinction ratio, the "projection operators" for Bob's measurements will actually comprise a projector mixed with a very small (≈ 0.01) amount of the identity operator. This can only ever decrease the correlation with Alice's results, so if Bob takes this effect into account, it can only be to Alice's benefit, by making it easier for her to convince him that she is steering his state. Therefore, to subject our demonstration of steering to the highest level of rigour, we can ignore this imperfection. The second sort of imperfection is that the true states onto which Bob projects, corresponding to vectors $\tilde{\mathbf{u}}_k$ and $-\tilde{\mathbf{u}}'_k$ on the Bloch sphere, differ slightly from \mathbf{u}_k and $-\mathbf{u}_k$ respectively. Note also that in our experiment Bob used only one detector, for reasons of space efficiency; thus he needs to implement two different projections for each choice of setting k , and hence $\tilde{\mathbf{u}}'_k$ is not necessarily equal to $\tilde{\mathbf{u}}_k$. These errors arise from Bob's inability to perform rotations on the Bloch sphere to arbitrary accuracy, for the following reasons: a. due to imperfect alignment of the optic axis of his wave plates (QWP and HWP) with projection axis ($\hat{\sigma}_Z$) of the PBS, b. the repeatability error in the motorised stages (setting the angles of both wave plates), and c. due to wave plate imperfections – their polarisation retardance is quoted only to within $\pm\pi/250$. The magnitudes of all of these errors is systematically determined, and a Monte Carlo simulation including all of the aforementioned factors allows us to determine the maximum infidelity of Bob's actual measurements ($\tilde{\mathbf{u}}_k$) with his ideal measurements (\mathbf{u}_k). Unlike the error due to a finite PBS extinction ratio, Bob's measurement misalignment can, in principle, make it easier for Alice to fake steering his state. Therefore it is essential to bound the error in our measured \mathcal{S}_n due to this sort of error.

Because Bob only uses a single detector, we define the outcome $B_k = +1$ as being Bob getting a photon and "discovering" that he was projecting in the direction $\tilde{\mathbf{u}}_k$, and $B_k = -1$ likewise but projecting in the direction $-\tilde{\mathbf{u}}'_k$. Provided (as is the case) that Bob chooses to project in the directions $\tilde{\mathbf{u}}_k$ and $-\tilde{\mathbf{u}}'_k$ with equal probability, if there were no misalignment errors then the rate of occurrence of the event " $B_k = +1$ or $B_k = -1$ " would be independent of Alice's results. But in the nonideal situation we cannot make that assumption. Therefore the observed probabilities $\tilde{P}(A_k, B_k)$ for the four possible coincidences (i.e. postselected on both Alice and Bob detecting a photon) are defined as

$$\tilde{P}(A_k, B_k = +1) = R_{\tilde{\mathbf{u}}_k}(A_k, B_k = +1)/\mathcal{R}_k, \quad \tilde{P}(A_k, B_k = -1) = R_{\tilde{\mathbf{u}}'_k}(A_k, B_k = -1)/\mathcal{R}_k, \quad (8)$$

$$\text{with } \mathcal{R}_k = \sum_{A_k = \pm 1} [R_{\tilde{\mathbf{u}}_k}(A_k, B_k = +1) + R_{\tilde{\mathbf{u}}'_k}(A_k, B_k = -1)]. \quad (9)$$

where R stands for the rate of the corresponding events occurring.

Let us represent the state Bob receives, conditioned on Alice's output $A_k = \pm 1$, by a vector $\mathbf{v}_{A_k}^B$ in the Bloch sphere, with $|\mathbf{v}_{A_k}^B| \leq 1$; note that these states do not depend on Bob's setup, $\tilde{\mathbf{u}}_k$ or $\tilde{\mathbf{u}}'_k$. The rates $R_{\tilde{\mathbf{u}}_k^{(\prime)}}(A_k, B_k)$ are then given by

$$R_{\tilde{\mathbf{u}}_k^{(\prime)}}(A_k, B_k) = R_{\tilde{\mathbf{u}}_k^{(\prime)}}(A_k) P_{\tilde{\mathbf{u}}_k^{(\prime)}}(B_k|A_k) \propto P_{\tilde{\mathbf{u}}_k^{(\prime)}}(A_k) \frac{1 + (-1)^{B_k} \tilde{\mathbf{u}}_k^{(\prime)} \cdot \mathbf{v}_{A_k}^B}{2}. \quad (10)$$

Note that Alice's marginal probabilities, $P_{\tilde{\mathbf{u}}_k^{(\prime)}}(A_k)$, normalized so that they sum to one for $A_k = \pm 1$, do not depend on Bob's measurement setup: $P_{\tilde{\mathbf{u}}_k}(A_k) = P_{\tilde{\mathbf{u}}'_k}(A_k) \equiv P(A_k)$; otherwise Bob could signal instantaneously to Alice. Note also that these may be slightly different from Alice's experimentally observed marginals $\tilde{P}(A_k)$ calculated from the full postselected distribution $\tilde{P}(A_k, B_k)$.

From equation (8) and equation (10), one can calculate the experimentally observed correlations $\tilde{E}_k = \langle A_k \tilde{\sigma}_k^B \rangle$

(corresponding to the actual measurement “ $\tilde{\sigma}_k^B$ ”, rather than the ideal one, $\hat{\sigma}_k^B$) to be

$$\tilde{E}_k \equiv \sum_{A_k, B_k} A_k B_k \tilde{P}(A_k, B_k) \quad (11)$$

$$= \left[P(A_k = +1) \frac{1 + \tilde{\mathbf{u}}_k \cdot \mathbf{v}_{A_k=+1}^B}{2} - P(A_k = -1) \frac{1 + \tilde{\mathbf{u}}_k \cdot \mathbf{v}_{A_k=-1}^B}{2} \right. \\ \left. - P(A_k = +1) \frac{1 - \tilde{\mathbf{u}}'_k \cdot \mathbf{v}_{A_k=+1}^B}{2} + P(A_k = -1) \frac{1 - \tilde{\mathbf{u}}'_k \cdot \mathbf{v}_{A_k=-1}^B}{2} \right] / \mathcal{N}_k. \quad (12)$$

Here \mathcal{N}_k is defined so that the four terms above (without the minus signs) sum to one. Defining

$$\bar{\mathbf{u}}_k \equiv (\tilde{\mathbf{u}}_k + \tilde{\mathbf{u}}'_k) / 2, \quad (13)$$

$$\delta \mathbf{u}_k \equiv (\tilde{\mathbf{u}}_k - \tilde{\mathbf{u}}'_k) / 2, \quad (14)$$

$$\bar{\mathbf{v}}_k \equiv P(A_k = +1) \mathbf{v}_{A_k=+1}^B - P(A_k = -1) \mathbf{v}_{A_k=-1}^B, \quad (15)$$

$$\delta \mathbf{v}_k \equiv P(A_k = +1) \mathbf{v}_{A_k=+1}^B + P(A_k = -1) \mathbf{v}_{A_k=-1}^B, \quad (16)$$

we can rewrite \tilde{E}_k more simply as

$$\tilde{E}_k = \bar{\mathbf{u}}_k \cdot \bar{\mathbf{v}}_k / \mathcal{N}_k \quad \text{with} \quad \mathcal{N}_k = 1 + \delta \mathbf{u}_k \cdot \delta \mathbf{v}_k, \quad (17)$$

while the “true value” E_k of the correlation $\langle A_k \hat{\sigma}_k^B \rangle$ (corresponding now to the ideal measurement settings $\pm \mathbf{u}_k$) is simply $E_k = \mathbf{u}_k \cdot \bar{\mathbf{v}}_k$.

In order to quantify the deviation of \tilde{E}_k from its “true value” E_k , we characterize the misalignment of the vectors $\tilde{\mathbf{u}}_k^{(i)}$ by their scalar product with \mathbf{u}_k , the ideal setting: $\tilde{\mathbf{u}}_k^{(i)} \cdot \mathbf{u}_k \equiv \chi_k^{(i)}$. Further, we assume that we can bound the misalignment by $\chi_k^{(i)} \geq X_k > 0$, for some X_k less than, but close to, unity. One can then immediately prove the following, which will be useful later:

$$|\bar{\mathbf{u}}_k|^2 + |\delta \bar{\mathbf{u}}_k|^2 = 1; \quad X_k^2 \leq |\bar{\mathbf{u}}_k|^2 \leq 1 \quad \text{and} \quad 0 \leq |\delta \bar{\mathbf{u}}_k|^2 \leq 1 - X_k^2. \quad (18)$$

Let us start by bounding the normalisation coefficient \mathcal{N}_k . For that, first note that $|\bar{\mathbf{v}}_k|, |\delta \mathbf{v}_k| \leq 1$, and

$$|\bar{\mathbf{v}}_k|^2 + |\delta \mathbf{v}_k|^2 = 2 P(A_k = +1)^2 |\mathbf{v}_{A_k=+1}^B|^2 + 2 P(A_k = -1)^2 |\mathbf{v}_{A_k=-1}^B|^2, \quad (19)$$

$$\leq 2 P(A_k = +1)^2 + 2 P(A_k = -1)^2 = 1 + (\delta P_k^A)^2, \quad (20)$$

where $\delta P_k^A \equiv P(A_k = +1) - P(A_k = -1)$. Defining in a similar way $\delta \tilde{P}_k^A \equiv \tilde{P}(A_k = +1) - \tilde{P}(A_k = -1)$, we find, using equation (12), $\mathcal{N}_k \delta \tilde{P}_k^A = \delta P_k^A + \delta \mathbf{u}_k \cdot \bar{\mathbf{v}}_k$. Besides, from equation (17) we have $|\bar{\mathbf{u}}_k| |\bar{\mathbf{v}}_k| \geq \mathcal{N}_k \tilde{E}_k$. Hence, following on equation (20),

$$|\delta \mathbf{v}_k|^2 \leq 1 + (\mathcal{N}_k \delta \tilde{P}_k^A - \delta \mathbf{u}_k \cdot \bar{\mathbf{v}}_k)^2 - |\bar{\mathbf{v}}_k|^2 \quad (21)$$

$$\leq 1 + \mathcal{N}_k^2 (\delta \tilde{P}_k^A)^2 + 2 \mathcal{N}_k |\delta \tilde{P}_k^A| |\delta \mathbf{u}_k| |\bar{\mathbf{v}}_k| - |\bar{\mathbf{u}}_k|^2 |\bar{\mathbf{v}}_k|^2 \quad (22)$$

$$\leq 1 + 2 \mathcal{N}_k |\delta \tilde{P}_k^A| \sqrt{1 - X_k^2} - \mathcal{N}_k^2 [\tilde{E}_k^2 - (\delta \tilde{P}_k^A)^2]. \quad (23)$$

Now, for typical experimental values, the previous expression decreases with \mathcal{N}_k . From equations (17) and (18), we have $\mathcal{N}_k \geq 1 - |\delta \mathbf{u}_k| |\delta \mathbf{v}_k| \geq 1 - \sqrt{1 - X_k^2} |\delta \mathbf{v}_k|$, so that we get

$$|\delta \mathbf{v}_k|^2 \leq 1 + 2 \left(1 - \sqrt{1 - X_k^2} |\delta \mathbf{v}_k| \right) |\delta \tilde{P}_k^A| \sqrt{1 - X_k^2} - \left(1 - \sqrt{1 - X_k^2} |\delta \mathbf{v}_k| \right)^2 [\tilde{E}_k^2 - (\delta \tilde{P}_k^A)^2] \quad (24)$$

$$\leq 1 - \tilde{E}_k^2 + (\delta \tilde{P}_k^A)^2 + 2 |\delta \tilde{P}_k^A| \sqrt{1 - X_k^2} + 2 \sqrt{1 - X_k^2} \tilde{E}_k^2 |\delta \mathbf{v}_k|, \quad (25)$$

where the negative terms we discarded are negligible for our experimental parameters, so do essentially not affect the tightness of the above bound. By resolving the quadratic equation in $|\delta \mathbf{v}_k|$ above, we further obtain

$$|\delta \mathbf{v}_k| \leq \sqrt{1 - X_k^2} \tilde{E}_k^2 + \sqrt{(1 - X_k^2) \tilde{E}_k^4 + 1 - \tilde{E}_k^2 + (\delta \tilde{P}_k^A)^2 + 2 |\delta \tilde{P}_k^A| \sqrt{1 - X_k^2}}, \quad (26)$$

which involves only terms obtainable from experimental data. Substituting back into equation (17) we obtain $|\mathcal{N}_k - 1| \leq \delta\mathcal{N}_k$, where

$$\delta\mathcal{N}_k \equiv \left[\sqrt{1 - X_k^2} \tilde{E}_k^2 + \sqrt{(1 - X_k^2) \tilde{E}_k^4 + 1 - \tilde{E}_k^2 + (\delta\tilde{P}_k^A)^2 + 2|\delta\tilde{P}_k^A| \sqrt{1 - X_k^2}} \right] \sqrt{1 - X_k^2}. \quad (27)$$

Let us now decompose the vectors \mathbf{u}_k and \mathbf{v}_k onto $\bar{\mathbf{u}}_k$:

$$\mathbf{u}_k = \frac{\chi_k + \chi'_k}{2|\bar{\mathbf{u}}_k|} \frac{\bar{\mathbf{u}}_k}{|\bar{\mathbf{u}}_k|} + \sqrt{1 - \frac{(\chi_k + \chi'_k)^2}{4|\bar{\mathbf{u}}_k|^2}} \bar{\mathbf{u}}_k^{\perp,u} \quad (28)$$

$$\mathbf{v}_k = \frac{\mathcal{N}_k \tilde{E}_k}{|\bar{\mathbf{u}}_k|} \frac{\bar{\mathbf{u}}_k}{|\bar{\mathbf{u}}_k|} + \sqrt{|\bar{\mathbf{v}}_k|^2 - \frac{\mathcal{N}_k^2 \tilde{E}_k^2}{|\bar{\mathbf{u}}_k|^2}} \bar{\mathbf{u}}_k^{\perp,v} \quad (29)$$

where $\bar{\mathbf{u}}_k^{\perp,u}$ and $\bar{\mathbf{u}}_k^{\perp,v}$ are two unit vectors on the Bloch sphere, both orthogonal to $\bar{\mathbf{u}}_k$. One then gets

$$\Delta E_k \equiv |E_k - \tilde{E}_k| = |\mathbf{u}_k \cdot \mathbf{v}_k - \tilde{E}_k| \quad (30)$$

$$= \left| \frac{\chi_k + \chi'_k}{2|\bar{\mathbf{u}}_k|} \frac{\mathcal{N}_k \tilde{E}_k}{|\bar{\mathbf{u}}_k|} - \tilde{E}_k + \sqrt{1 - \frac{(\chi_k + \chi'_k)^2}{4|\bar{\mathbf{u}}_k|^2}} \sqrt{|\bar{\mathbf{v}}_k|^2 - \frac{\mathcal{N}_k^2 \tilde{E}_k^2}{|\bar{\mathbf{u}}_k|^2}} \bar{\mathbf{u}}_k^{\perp,u} \cdot \bar{\mathbf{u}}_k^{\perp,v} \right| \quad (31)$$

$$\leq \left| \frac{\chi_k + \chi'_k}{2} \frac{\mathcal{N}_k}{|\bar{\mathbf{u}}_k|^2} - 1 \right| |\tilde{E}_k| + \sqrt{1 - X_k^2} \sqrt{1 - \mathcal{N}_k^2 \tilde{E}_k^2}. \quad (32)$$

To bound this further, one can show that $X_k \leq (\chi_k + \chi'_k)/2|\bar{\mathbf{u}}_k|^2 \leq 1/X_k$. Using the bound on \mathcal{N}_k derived above, we finally obtain

$$\Delta E_k \leq (1 - X_k + \delta\mathcal{N}_k) |\tilde{E}_k| / X_k + \sqrt{1 - X_k} \sqrt{1 - (1 - \delta\mathcal{N}_k)^2 \tilde{E}_k^2}, \quad (33)$$

where all of these quantities are experimentally defined. Because systematic errors may not be independent, we add them linearly to obtain the total systematic error in \mathcal{S}_n to be at most

$$\Delta\mathcal{S}_n(\text{systematic}) = \frac{1}{n} \sum_k \left[(1 - X_k + \delta\mathcal{N}_k) |\tilde{E}_k| / X_k + \sqrt{1 - X_k} \sqrt{1 - (1 - \delta\mathcal{N}_k)^2 \tilde{E}_k^2} \right]. \quad (34)$$

The size of the different components of this systematic error can be seen in Tables I and II. The indicative sizes of the basic experimental parameters used to calculate the systematic error (they vary only slightly with n and k) are: $\tilde{E}_k \approx 0.99$, $1 - X_k \approx 2 \times 10^{-4}$, and $|\delta\tilde{P}_k^A| \approx 0.02$, implying $\delta\mathcal{N}_k \approx 0.002$.

TABLE I: Size of error factors contributing to $\Delta\mathcal{S}_n(\text{systematic})$ — Fig. 5 data — without 1 km fiber

n	$\Delta\mathcal{S}_n(\text{systematic})$	$\frac{1}{n} \sum (1 - X_k + \delta\mathcal{N}_k) \tilde{E}_k / X_k$	$\frac{1}{n} \sum \sqrt{1 - X_k} \sqrt{1 - (1 - \delta\mathcal{N}_k)^2 \tilde{E}_k^2}$
$n = 3$	0.0049	0.00290	0.00195
$n = 4$	0.0052	0.00311	0.00206
$n = 6$	0.0045	0.00272	0.00182
$n = 10$	0.0045	0.00270	0.00180
$n = 16$	0.0046	0.00277	0.00185

Experimental error calculation, part 2: statistical error

The statistical error component $\Delta\mathcal{S}_n(\text{statistical})$ in the total error $\Delta\mathcal{S}_n$ is a result of having a finite ensemble size. The error in the total number of Alice–Bob coincident events N_c is $\pm\sqrt{N_c}$, as governed by Poissonian statistics. The error $\Delta\mathcal{S}_n(\text{statistical})$ is determined by simply propagating the error in the counting errors through to the calculation of the joint probabilities $\langle A_k \hat{\sigma}_k^B \rangle$. This propagation provides the value $\Delta\langle A_k \hat{\sigma}_k^B \rangle$, and each of these terms contribute in quadrature to $\Delta\mathcal{S}_n(\text{statistical})$.

TABLE II: Size of error factors contributing to $\Delta\mathcal{S}_n(\text{systematic})$ — Fig. 5 data — with 1 km fiber

n	$\Delta\mathcal{S}_n(\text{systematic})$	$\frac{1}{n} \sum (1 - X_k + \delta\mathcal{N}_k) \tilde{E}_k / X_k$	$\frac{1}{n} \sum \sqrt{1 - X_k} \sqrt{1 - (1 - \delta\mathcal{N}_k)^2 \tilde{E}_k^2}$
$n = 10$	0.0057	0.00339	0.00232
$n = 16$	0.0063	0.00370	0.00256

Experimental error calculation, part 3: total error

Combining the statistical error with the systematic error derived before, we calculate the error in the experimental value of \mathcal{S}_n as

$$\Delta\mathcal{S}_n = \sqrt{\Delta\mathcal{S}_n(\text{systematic})^2 + \Delta\mathcal{S}_n(\text{statistical})^2}.$$

The magnitude of both the systematic ($\Delta\mathcal{S}_n(\text{systematic})$) and statistical ($\Delta\mathcal{S}_n(\text{statistical})$) errors in the data presented in Fig. 5 is shown in Tables III and IV.

TABLE III: Size of systematic and statistical error factors contributing to $\Delta\mathcal{S}_n$ — Fig. 5 data — without 1 km fiber

n	\mathcal{S}_n	$\Delta\mathcal{S}_n$	$\Delta\mathcal{S}_n(\text{systematic})$	$\Delta\mathcal{S}_n(\text{statistical})$
$n = 3$	0.989	0.0053	0.0048	0.0022
$n = 4$	0.990	0.0059	0.0052	0.0029
$n = 6$	0.990	0.0051	0.0045	0.0023
$n = 10$	0.991	0.0049	0.0045	0.0019
$n = 16$	0.991	0.0048	0.0046	0.0015

TABLE IV: Size of systematic and statistical error factors contributing to $\Delta\mathcal{S}_n$ — Figure 5 data — with 1 km fiber

n	\mathcal{S}_n	$\Delta\mathcal{S}_n$	$\Delta\mathcal{S}_n(\text{systematic})$	$\Delta\mathcal{S}_n(\text{statistical})$
$n = 10$	0.9847	0.0063	0.0057	0.0028
$n = 16$	0.9805	0.0067	0.0063	0.0023